Environmental Science Nano

Sulfolipid density dictates the extent of carbon nanodot interaction with chloroplast membranes

Journal:	*Environmental Science: Nano*
Manuscript ID	EN-ART-02-2022-000158.R1
Article Type:	Paper

SCHOLARONE™
Manuscripts

ENVIRONMENTAL SIGNIFICANCE STATEMENT

Interest in agricultural application of nanomaterials has risen due to their ability to target and control the delivery of agrochemicals, genetic elements, and biomolecules. Underlying nanomaterial interaction mechanisms with plant cell organelles is still in its infancy. Addressing plant organelle-nanoparticle interactions knowledge gaps is essential to design sustainable nanomaterials with targeted delivery functionality. Carbon nanodots are emerging as nanomaterials with a variety of applications in agriculture. In this study, we demonstrate that the molecular level interaction of carbon nanodots with chloroplast membranes is governed by the density of sulfolipid in the membrane *via* electrostatics. Our study contributes to determining structure-property-interaction relationships between nanomaterials and chloroplast membranes for enhancing or controlling plant function.

Sulfolipid density dictates the extent of carbon nanodot interaction with chloroplast membranes

Kyoungtea Kim,[a,1] Su-Ji Jeon,[b] Peiguang Hu,[b,2] Caroline M. Anastasia,[c] William F. Beimers,[d,3] Juan Pablo Giraldo,[*,b] and Joel A. Pedersen[*,a,c,e,4]

[a] Molecular and Environmental Toxicology, University of Wisconsin—Madison, Madison, Wisconsin 53706, United States
[b] Department of Botany and Plant Sciences, University of California—Riverside, Riverside, California 92521, United States
[c] Department of Chemistry, University of Wisconsin—Madison, Madison, Wisconsin 53706, United States
[d] Department of Chemistry, St. Olaf College, Northfield, Minnesota 55057, United States
[e] Departments of Soil Science and Civil & Environmental Engineering, University of Wisconsin—Madison, Madison, Wisconsin 53706, United States
[1] Present address: Eshelman School of Pharmacy, University of North Carolina at Chapel Hill, Chapel Hill, North Carolina 27599, United States
[2] Present address: Westwood Bioscience, Los Angeles, California 90025, United States
[3] Present address: Department of Biochemistry, University of Wisconsin—Madison, Madison, Wisconsin 53706, United States
[4] Present address: Department of Environmental Health and Engineering, Johns Hopkins University, Baltimore, Maryland 21218, United States

ABSTRACT

Mechanisms of nanomaterial delivery to plant chloroplasts have been explored to improve plant stress tolerance, promote photosynthesis, facilitate genetic engineering, and manufacture self-repairing biomaterials, fuels, and biopharmaceuticals. However, the molecular interactions of nanomaterials with chloroplast membranes are not well understood. In this study, we examine the interactions of an important set of chloroplast membrane lipids including sulfoquinovosyl diacylglycerols with carbon nanodots varying in functional group charge. To accomplish this objective, we constructed a novel model chloroplast membrane and interrogated the influence of carbon nanodot functional group charge, model chloroplast membrane composition, and ionic strength on the carbon nanodot-chloroplast membrane interactions using quartz crystal microbalance with dissipation monitoring. We further examined the interaction of carbon nanodots with native chloroplasts isolated from *Arabidopsis thaliana* using confocal laser-scanning

microscopy. Our results indicate that carbon nanodot–chloroplast membrane interactions are dictated primarily by electrostatics. Despite being the least abundant lipids in chloroplast membranes, we find that the relative abundance of sulfoquinovosyl diacylglycerol in model membranes is a critical factor governing both the affinity and capacity of the membrane for positively charged carbon nanodots. Rates of carbon nanodot attachment to model chloroplast membranes varied with ionic strength in a manner consistent with electrical double layer compression on carbon nanodots. Our findings elucidate chemical interactions between nanomaterials and plant biosurfaces at the molecular level and potentially contribute to establishing structure–property–interaction relationships of sustainable nanomaterials with plant organelle membranes.

Keywords: Structure–property–interaction relationships, quartz crystal microbalance with dissipation monitoring, confocal microscopy, carbon dots, nanoparticle-plant interactions, chloroplast membranes

INTRODUCTION

Distinctive physicochemical properties of nanomaterials (NMs), such as small size, tunable surface charge, morphology, high surface area, and the ability to encapsulate and deliver cargos *via* surface modifications offer potential to act as a tool to improve agriculture.[1] The small size of NMs plays a pivotal role in cargo delivery by allowing movement through biological barriers.[2] Charge and morphology of NMs have also been shown to influence translocation and distribution in plants.[2,3] The chemical composition of the NM surface also dictates cellular uptake pathways, leading to variable translocation and uptake in cells or organisms.[4] Previous studies have exploited the tunable surface properties of NMs to improve the efficacy in delivering chemical cargoes or genetic materials to plant cell organelles.[5,6]

Nanomaterial-mediated agrochemical and gene delivery are expected to overcome some of the limitations of established chemical and genetic engineering approaches to improve plant performance, including low efficiency, lack of targeted and controlled delivery, unexpected adverse impacts, and limitation of general use to tractable plant species.[7,8] Employment of NMs in agrochemical formulations has been shown to increase permeability and translocation, potentially overcoming barriers in the efficacy of traditional fertilizers.[4,9] Enhanced cargo capacity and delivery efficiencies for genetic molecules have been achieved by polymer functionalization of NMs. For instance, positively charged polyethyleneimine (PEI) is one of the widely used polymers to coordinate negatively charged genetic materials with NMs *via* electrostatic interactions.[10,11] Polyethyleneimine-functionalized NMs have been shown to transfer genetic material cargoes into pollen[12] and nucleus[13] followed by modified or enhanced gene expressions. Despite these advances on NM-cargo interactions, a large part of NM–plant cell/organelle interactions at the molecular level remains unexplored.[14,15]

Since chloroplasts play a pivotal role in a wide range of plant metabolism pathways including the regulation of crop yields and plant growth and yield,[16] they serve as a promising target organelle for NM based gene editing of plants.[5] Interfacing NMs with chloroplasts has been demonstrated to enhance photosynthesis by augmenting the light-harvesting system[8,15,17] and promoting electron transport.[8] Chloroplasts also have been widely studied as platforms for improving plant performance through genetic engineering, due to the possession of their own small prokaryotic type genome, lack of gene silencing, and high level of expression of transgenes.[18–21] Gene delivery by NMs could be a cost-effective, efficient, and generic method to facilitate chloroplast transformation, without physical damage on plant tissues.[21,22] Such applications have

promoted rational design of NMs to improve targeting and gene delivery ability to chloroplasts.[5,22,23]

Between 52 and 84% of chloroplast membranes consist of unique classes of galactolipids and sulfolipid: monogalactosyldiacylglycerol (MGDG), digalactosyldiacylglycerol (DGDG), and sulfoquinovosyldiacylglycerol (SQDG).[24] Sulfoquinovosyldiacylglycerol is one of the most distinct classes of lipids found in photosynthetic apparatuses: phytoflagellates, cyanobacteria, purple sulfur and non-sulfur bacteria, algae, and all photosynthetic plants.[25] They are predominantly distributed in plastid membranes, and their sulphonic acid on head groups lead to stable and strong acidity over a wide range of pH.[25,26] Due to its acidic head group, SQDG is considered to play an important biological role in balancing anionic charge over the membrane.[27] A large portion of SQDG in the membrane of photosynthetic apparatus is unsaturated and has an acyl chain length of 14 to 22 carbons.[28] Another characteristic class of lipids is galactolipids found in thylakoid membranes from higher plants.[16] The most abundant lipid components of galactolipids are electroneutral MGDG and DGDG, which contain one and two galactoses as their head groups, respectively.[24] Both galactolipids consist mostly of unsaturated 18 carbon-long acyl chains, which allows structural integrity and fluidity of the thylakoid membrane at physiological temperature range.[29–31] Although lipid composition varies depending on plant species, MGDG and DGDG constitute up to 49% and 30% of chloroplast membrane, respectively, while SQDG makes up 5-7% of chloroplast membrane lipids.[9,29,32,33]

Carbon nanodots (CNDs) are a newly emerging carbon based NM[34] and regarded as a promising NM for applications in agriculture.[2] Their small size, typically below 10 nm,[34] allows facile penetration through plant cell walls having size-exclusion limits of 20-40 nm.[21] Carbon nanodots are also amenable to surface modification,[35] which can grant both high water solubility

and allow for entry into plant cells.[21,36] Control over these physicochemical properties provides a framework for optimization of plant cell uptake, since size and surface charge of CNDs is known to impact plant cell uptake pathway, distribution, and biocompatibility.[37,38] Tunable surface modification is expected to enable targeted delivery of cargo molecules to specific cells and organelles.[34] Another advantage of CND application is that they are trackable due to their intrinsic fluorescence capabilities, making them well-suited for bioimaging *in vitro* or *in vivo*.[36,39]

In this study, we hypothesized that electrostatics play a critical role in CND interaction with chloroplast membranes. Because SQDG has a negatively charged head group, we anticipate that positively charged CNDs will have preferential interaction with SQDG rather than uncharged galactolipids/phospholipids. We developed an *in vitro* model planar surfaces for outer chloroplast membranes and use them to determine molecular-level interactions between CNDs and chloroplast membranes. Additionally, we use these model membranes to evaluate the role of the anionic chloroplast lipid SQDG in interactions with CNDs of varying charge. We fabricated model chloroplast membranes containing a range of SQDG concentrations and evaluated the extent of their interactions with CNDs using quartz crystal microbalance with dissipation monitoring (QCM-D). We also tested the influence of ionic strength on both CND–membrane and CND–CND interactions. The affinity of CNDs for chloroplast membranes was further evaluated by confocal microscopy using chloroplasts isolated from *Arabidopsis thaliana*. The model planar membranes reflect characteristic lipid compositions of chloroplasts and act as a tool for assessing NM interaction with plant organelle membranes and developing structure–property–interaction relationships of NMs with chloroplast membranes.

MATERIALS AND METHODS

Materials. We purchased Soy PC (> 99%), MGDG (> 99%), DGDG (> 99%), and SQDG (> 99%) from Avanti polar lipids (Albaster, AL, USA). Magnesium dichloride (≥ 99.99%), and chloroform (> 99.8%) were obtained from MilliporeSigma (Burlington, MA, USA). We acquired 2-[4-(2-hydroxyethyl)piperazin-1-yl]ethanesulfonic acid (HEPES) and sodium dodecyl sulfate (SDS) from DOT scientific (Burton, MI, USA). Ultrapure water (resistivity 18.2 MΩ·cm) was produced by a GenPure Pro UV-TOC/UF system (Thermo Fisher Scientific, Waltham, MA, USA). All solutions were buffered to pH 7.5 with 0.010 M HEPES and ionic strength was adjusted by the addition of potassium chloride (≥ 99.999%, Thermo Fisher Scientific, Waltham, MA, USA). For CND syntheses, we purchased citric acid (99.7%), urea (99.2%), ethanol (96%), and chloroform from Thermo Fisher Scientific (Waltham, MA, USA). We acquired sodium hydroxide, ammonium hydroxide ($NH_3 \cdot H_2O$, 30–33%), N,N-Dimethylformamide (DMF, > 99%), and 0.22 μm syringe filters from MilliporeSigma (Burlington, MA, USA). Polyethyleneimine (branched, M.W. ~10k), polyvinylpyrrolidone (M.W. ~10k), and succinic anhydride (99%) were obtained from Alfa Aesar (Haverhill, MA, USA).

Synthesis of CNDs. Three differently charged CNDs were synthesized by following previously reported protocols with modifications.[2] The CND cores were made by hydrothermal reactions using citric acid, urea, and ammonium hydroxide mixtures. In brief, 1.92 g of citric acid and 2.40 g of urea were dissolved in 2 mL of ultrapure water and 1.35 mL of ammonium hydroxide ($NH_3 \cdot H_2O$, 30–33%) was added into the mixture. The mixture was reacted at 180 °C for 1.5 h and was cooled down to room temperature and redissolved in ultrapure water. The aggregate was removed by centrifugation at 3082 ×g for 30 min. To remove fluorescence by-products, the CNDs were purified by dialysis (MWCO 1k, Spectra/Por® 6 Standard Dialysis Tubing, Spectrum

Chemical Mfg. Corp., New Brunswick, NJ, USA) until there was no significant absorbance or fluorescence of the dialysate (Fig. S1). The solution was further filtered with a syringe filter (pore size 0.02 μm) to obtain nanosized CND cores. To functionalize CND cores with PEI, a 16 mL CND solution (5 $mg \cdot mL^{-1}$) was added to a 20 mL glass vial and the pH adjusted to 12 with NaOH. This CND suspension was added to 3.2 mL PEI solution (0.1 $g \cdot mL^{-1}$) while vigorously stirring and reacted at 85 ℃ for 16 h. The solution was cooled down and purified by mixing with ethanol and chloroform (1:1 v/v). To separate aqueous phase from organic solvent phase, we centrifuged the solution at 3905 ×g for 5 min. This purification step was repeated five times. The purified PEI-CND solution was air-dried to remove organic solvent residuals. Polyvinylpyrrolidone coated CNDs (PVP-CNDs) were produced in the same manner except that purification was performed with a mixture of acetone and chloroform. The carboxylated polyethyleneimine CNDs (CP-CNDs) were synthesized by the modification of PEI-CNDs upon reaction with succinic anhydride. Briefly, 15 mL of succinic anhydride dissolved in DMF was added rapidly to 30 mL of PEI-CNDs solution (1 $mg \cdot mL^{-1}$) and stirred at room temperature overnight. Once CP-CND synthesis was finished, the final product was purified the same way as PEI-CNDs.

Characterization of CNDs. Transmission electron microscopy (TEM) images were obtained on a Philips FEI Tecnai 12 microscope (Philips, Amsterdam, Netherlands) operated at an accelerating voltage of 120 kV. One drop of particle solution was placed onto a Cu grid (400 mesh, Ted Pella) for TEM imaging. The UV–Vis absorption spectra of CNDs were determined using a micro quartz cuvette (10 mm × 2 mm, path length 10 mm) using a Shimadzu UV-2600 spectrometer (Shimadzu, Kyoto, Japan). Fluorescence spectra of CNDs were measured using a 10 mm × 10 mm PTI QuantaMaster 400 fluorophotometer quartz cuvettes (Horiba, Kyoto, Japan). X-ray photoelectron spectroscopy (XPS) was performed using a Kratos AXIS ULTRADLD XPS

system equipped with an Al Ka X-ray source and a 165-mm mean radius electron energy hemispherical analyzer.

The relative fluorescence quantum yield of PEI-CND used for confocal microscopy analysis was measured by using quinine sulfate in 0.1 M H_2SO_4 as a standard and the following equation:[40,41]

$$Q_{CND} = Q_{QS} \times \frac{I_{CND}}{I_{QS}} \times \frac{A_{QS}}{A_{CND}} \times \frac{{\eta_{CND}}^2}{{\eta_{QS}}^2} \quad \text{Eq. (1)}$$

where Q_{CND} = quantum yield of CND, Q_{QS} = quantum yield of quinine sulfate, I_{CND} = integrated fluorescence intensity of CND, I_{QS} = integrated fluorescence intensity of quinine sulfate, A_{QS} = absorbance of quinine sulfate, A_{CND} = absorbance of CND, η_{CND} = refractive index of CND, η_{QS} = refractive index of quinine sulfate. The quantum yield of quinine sulfate in 0.1 M H_2SO_4 is 0.54 and the refractive index of water is 1.33.

Lipid Vesicle Preparation and Characterization. Lipids were received as a powder and dissolved in chloroform to a final concentration of 1 mg·mL^{-1}. Stock solutions were stored at –20 °C in the dark and used within 2 weeks. Small unilamellar vesicles were prepared by the extrusion method.[42] Briefly, the stock lipid solutions were mixed to the desired molar ratios in glass vials, and the solvent was evaporated under nitrogen flow. To remove residual solvent, the vials remained under vacuum in the dark overnight. Afterward, the dried lipid mixtures were rehydrated by suspending in 10 mM $MgCl_2$ buffered to pH 7.5 with 10 mM HEPES by brief vortexing followed by sonication until opaque (5 min). The suspensions were snap-frozen in liquid nitrogen and thawed by another 5 min of sonication. Following three freeze-thaw cycles, the suspensions were extruded 21 times through polycarbonate membranes (0.1 μm pore size, 19 mm diameter, Whatman, Maidstone, UK) with a 610000 extruder kit (Avanti Polar Lipids, Albaster,

AL, USA). Prepared vesicles were stored at 4 °C and used within 12 h. The hydrodynamic diameters (d_h) and zeta potential (ζ) of the vesicles were determined by dynamic light scattering and laser Doppler microelectrophoresis at 25 °C (Zetasizer Nano DS, Malvern Panalytical, Malvern, UK). Vesicle characteristics are shown in Fig. 1.

Preparation of Solid-Supported Bilayers and Carbon Nanodots – Model Chloroplast Membrane Interactions. We procured SiO_2-coated QCM-D sensors (QSX 303) from Biolin Scientific (Gothenburg, Sweden). All solutions for QCM-D experiment were passed through 0.22 μm syringe filters (MilliporeSigma, Burlington, MA, USA) prior to each experiment. Prior to the experiment, QCM-D sensors were cleaned with 2 wt. % sodium dodecyl sulfate (SDS) solution and UV/Ozone cleaner (Bioforce Nanosciences UV/Ozone Procleaner, Bioforce Nanosciences, Salt Lake City, UT, USA) per manufacturer recommendations. Briefly, sensors were immersed in 2% SDS solution for 30 min at room temperature and then thoroughly rinsed with ultrapure water. Sensors were dried under nitrogen gas flow and exposed to UV/ozone for 10 min. The cleaned sensors were mounted on Q-Sense flow modules (QFM 401, Biolin Scientific, Gothenburg, Sweden) with a Q-sense system (E4, Biolin Scientific, Gothenburg, Sweden). The sensor surfaces were equilibrated under a flow of 0.010 M $MgCl_2$ solution buffered to pH 7.5 with 0.010 M HEPES. Equilibration was finished when f_n did not change more than ± 0.5 Hz over 30 m. Model chloroplast membranes were constructed using the vesicle fusion method.[43] Figure S1 shows a representative QCM-D trace for a model chloroplast bilayer formation and subsequent interaction with CNDs. Flow rate of all buffers and solutions were maintained at a constant rate of 0.100 $mL \cdot min^{-1}$ for the entire experiment.

Quartz crystal microbalance with dissipation (QCM-D) monitoring. We measured changes in frequency (Δf_n) and energy dissipation (ΔD_n) of model systems upon CND

exposure to elucidate the impact of CND on model chloroplast membranes. Rigidity of model membranes was determined by the extent of energy dissipation at the interface defined as:[44]

$$D = \frac{E_{dissipated}}{2\pi E_{stored}} \quad \text{Eq. (2)}$$

where $E_{\text{dissipated}}$ is the energy dissipation per oscillation and E_{stored} is the energy stored in the system. Soft adlayers on QCM-D sensors induce decay of sensor oscillation when the electronic circuit is opened and subsequently lead to high energy dissipation. Rigid adlayers, on the contrary, do not drastically diminish sensor oscillation, thus they cause low energy dissipation.[44] As measured data for model membranes and CND-model membrane interactions had ratio of $\Delta D_n/(-\Delta f_n/n) \ll 4 \times 10^{-7}\ Hz^{-1}$ for 5 MHz crystal, which could be approximated as rigid adlayers,[45] the Sauerbrey equation (Eq. 2) was used to deduce acoustic mass densities ($\Gamma_{\text{QCM-D}}$).[44,46]

$$\Gamma_{QCM-D} = -C\frac{\Delta f_n}{n} \quad \text{Eq. (3)}$$

where n is the harmonic number and C is the mass sensitivity constant (18 ng·cm^{-2}·Hz^{-1}, for the sensors used in this study.) We here report $\Gamma_{\text{QCM-D}}$ and changes in energy dissipation (ΔD_n) of the 5$^{\text{th}}$ overtone (n = 5, *i.e.* ~25 MHz). Acoustic mass densities at or below the lower limit of detection of the QCM-D system (~1 ng cm^{-2} under our experimental settings)[47] was considered as zero.

Initial adsorption efficiencies (α) of CNDs onto the bilayers were approximated as:[48]

$$\alpha = \frac{(d\Gamma_{\text{QCM-D}}/dt)_{experimental}}{(d\Gamma_{\text{QCM-D}}/dt)_{theoretical}} \quad \text{Eq. (4)}$$

where $d\Gamma_{QCM\text{-}D}/dt$ refers to initial adsorption rate. Experimental $d\Gamma_{QCM\text{-}D}/dt$ was assessed from the first derivative of $\Gamma_{QCM\text{-}D}$ over the first 10 s of CND adsorption onto model membranes. Theoretical $d\Gamma_{QCM\text{-}D}/dt$ was calculated as follows:[49]

$$(d\Gamma_{\mathrm{QCM-D}}/dt)_{theoretical} = k_a m_s e^{-\left(k_a m_s/\Gamma^*\right)t} \quad \text{Eq. (5)}$$

where k_a is the rate constant of adsorption ($m \cdot s^{-1}$), m_s is the mass concentration of CND in bulk solution ($g \cdot m^{-3}$), and Γ^* is the maximum surface concentration of CND ($g \cdot m^{-2}$). Theoretical rate constant of adsorption, k_a, was determined as:[50]

$$k_a = D_c^{2/3} Q^{1/3} n \quad \text{Eq. (6)}$$

$$D_c = \frac{k_B T}{6\pi R \eta} \quad \text{Eq. (7)}$$

where D_c is the diffusion coefficient ($m^2 \cdot s^{-1}$) defined as Eq. 6, Q is the flow rate of fluid ($m^3 \cdot s^{-1}$), n is the geometrical constant of the system ($4.44 \times 10^3\ m^{-4/3}$), k_B is the Boltzmann constant ($m^2 \cdot kg \cdot s^{-2} \cdot K^{-1}$), T is the temperature (K), R is the radius of CND (m), and η is the viscosity of water ($kg \cdot m^{-1} \cdot s^{-1}$). The changes in frequencies were subjected to locally weighted scatterplot smoothing with a smoothing parameter of 0.1 as described previously.[51–53]

Fractional surface coverage area of CNDs (θ) of the model membranes upon CND exposure were calculated as the ratio of the occupied surface area by CNDs (A) to that of sensor surface area (S):

$$\theta = \frac{A}{S} = \frac{\pi R^2 \cdot n_{CND}}{S} \quad \text{Eq. (8)}$$

where S is 0.7854 (cm^2) for the experimental system used in this study and n_{CND} is the number of CNDs on the sensor. Because density of the CNDs used here is unknown, number of CNDs were

approximated on the assumption that the CNDs have a density between diamond at one extreme (~3.53 g·cm^{-3}) and polypropylene (~0.92 g·cm^{-3}) at the other extreme. In this study, the results based on this assumption is described as a range on the plots relevant for surface coverage. Number of CNDs at the interface was defined as:

$$n_{CD} = \frac{\Gamma_{QCM-D} \cdot S}{V \cdot \rho} \quad \text{Eq. (9)}$$

where V is the total volume of CNDs on the bilayers (cm^3) and ρ is the density of CNDs (g·cm^{-3}).

Particle adsorption in the initial stage was interpreted based on random sequential adsorption model.[54] According to the model, probability of additional N+1 particle adsorption is defined as:

$$p_{N+1} = \frac{S_A}{\Delta S} = 1 - \frac{S_B}{\Delta S} = 1 - S_B \quad \text{Eq. (10)}$$

where p_{N+1} is the probability of N+1 particle adsorption, S_A is the available surface area, S_B is the blocked (excluded) area by previously adsorbed particle, and ΔS is surface area of the entire interface. Since maximum surface coverage is dependent on ionic strength of milieu and lateral mobility of particles at interfaces,[55,56] we here described particle behavior in the initial stage of particle adsorption based on random sequential adsorption and fractional surface coverage, under various ionic strength of the experimental media.

Isolation of chloroplast from cells. Chloroplasts were isolated from 3-4 week-old Columbia ecotype (Col-0) *Arabidopsis thaliana* leaves (seed stock source CS60000) as previously described.[8] Chloroplasts isolation was performed in sucrose buffer (pH 7.3, 28 mM Na_2HPO_4, 22 mM KH_2PO_4, 2.5 mM $MgCl_2$, 400 mM sucrose, and 10 mM KCl) by chopping leaves using IKA benchtop A 10 Basic Mill (IKA-Werke, Staufen, Germany). Then samples were centrifuged at 3082 ×g for 10 min and separated in a Percoll gradient (1 mL layers of 80%, 60%, 40%, and 20%

Percoll in buffer). After centrifugation at 3082 ×g for 20 min, chloroplasts were selected from the 40% to 60% bands and washed. Concentration of chlorophyll was determined by an established method.[57] A 100 μL chloroplast solution was added to 1 mL of acetone-water mixture (8:2 v/v) to suspend chlorophyll molecules in chloroplasts, then vortexed and centrifuged at 3,000 ×g for 2 min. Absorbance of supernatant was determined at 652 nm and chlorophyll content calculated using an extinction coefficient of 0.036 $mg \cdot L^{-1} \cdot cm^{-1}$:

$$Abs = concentration\ of\ chlorophyll \times 36 \qquad \text{Eq. (11)}$$

For the confocal fluorescence imaging, 0.02 $mg \cdot mL^{-1}$ of chlorophyll mixture was prepared.

Microscopic Observance of CND-chloroplast interactions. Isolated chloroplast samples were imaged using a Zeiss inverted confocal microscope LSM 880 (Carl Zeiss, Jena, Germany).[2,5] Isolated chloroplast suspension in a 10 mM TES buffer (pH 7.4) was incubated with 0.1 $mg \cdot mL^{-1}$ of PEI-CND for 1 h. After incubation, the reaction mixture was washed with a 10 mM TES buffer solution (pH 7.4) to remove unbound PEI-CND by centrifugation (9300 ×g for 5 min). The chloroplast suspension was immediately placed on a glass slide with a chamber made with observation gel (Carolina, Burlington, NC, USA) for confocal analysis.[2,5] The imaging settings were as follows: ×40 wet objective (Zeiss Microsystems, Germany); 355 nm excitation for PEI-CND; 633 nm excitation for chloroplast. The photomultiplier tubes detection range was set 420–500 nm for PEI CND; 680−750 nm for chloroplasts.

Statistical Methods. The means in a series of experiments were compared using one-way analysis of variances (ANOVA) followed by *post hoc* comparison using the Tukey test (Prism ver. 9.0.2, GraphPad, San Diego, CA, USA). In figures, statistical significances among experimental groups are denoted by letters and their statistical significance is further described by asterisks in captions: $p \leq 0.05$ (*), $p \leq 0.01$ (**), $p \leq 0.001$ (***), and $p \leq 0.0001$ (****).

RESULTS AND DISCUSSION

Carbon nanodot interaction with model chloroplast membranes is influenced by sulfolipid content. SQDG is the only lipid containing a negative charge on its head group among major lipid components in the chloroplast membrane (Fig. 1a).[27] Thus, we hypothesized that the amount of SQDG plays an important role in the interaction of chloroplast membrane with charged CNDs via electrostatics. To examine the impact of SQDG content on the interactions of CNDs with model chloroplast membranes, we constructed lipid membranes containing different amounts of SQDG *via* the vesicle fusion method.[43] In chloroplast envelopes or thylakoid membranes of plants,[9,29,32,33] SQDG accounts for about 5-7% of total lipids; therefore, we constructed membranes containing 0, 2.5, 5, and 10% SQDG to examine the impact of both SQDG elimination and enrichment on the interactions with the CNDs. Since the model chloroplast membranes were prepared using the vesicle fusion method,[43] we measured the impact of SQDG amount on vesicle properties to further estimate the surface properties of the model membranes. Different amounts of SQDG had no significant impacts on the hydrodynamic diameters of the vesicles (Fig. 1b). Due to the sulfonic acid group on the head group of SQDG, higher abundance of SQDG leads to increased magnitude of the zeta-potential of the vesicles used to build model membranes (Fig. 1c) and a predicted decrease in the surface potential of the model membrane.

The extent of CND interaction with model chloroplast membranes was investigated with CNDs bearing three surface chemical compositions (Fig. 2) that were characterized through XPS (Fig. S2). Polyethylenimine (PEI) CNDs had positive apparent zeta potential, whereas carboxylated-PEI (CP) and polyvinylpyrrolidone (PVP) had negative apparent zeta potential under

the experimental conditions, pH 7.5. Zeta potentials and hydrodynamic diameters of three CNDs are shown in Fig. 2b-e. The magnitude of zeta-potential of the CNDs were inversely proportional to ionic strength due to electrical double layer compression (Fig. 2b-d).[58,59] The hydrodynamic diameters of the CNDs were independent of ionic strength in the range of 0 – 100 mM except for some aggregation of PVP-CNDs under no salt condition (Fig. 2e). The aggregation of PVP-CNDs could arise from the hydrophobic interactions of PVP polymers on particle surfaces under weak ionic strength of milieu.[60]

Model membranes containing 0, 2.5, 5, and 10 mol% SQDG were exposed to PEI-, CP-, or PVP-CNDs to compare the extent of CND adsorption under different ionic strengths. Association of the CNDs with model membranes was investigated in terms of affinity of CNDs for the model membranes and capacity of the membranes to accommodate CNDs. Affinity of CNDs to model membranes was determined from initial adsorption efficiencies in the initial stage of CND-membrane interaction (Fig. S3, early stage of #6). Once CND interaction with model membranes reached equilibrium (Fig. S3, later stage of #6), we calculated maximum acoustic mass densities ($\Gamma_{QCM\text{-}D}$) to evaluate maximum capacity of the membranes to accommodate CNDs.

Under our experimental conditions, only positively charged PEI-CNDs led to detectable attachment to SQDG containing model membranes (*cf.* Fig. S4 in the Supporting Information). The CP-CNDs having hydrophilic surface and PVP-CNDs having amphiphilic surface[61–63] did not induce any significant changes in mass density upon adsorption. These results indicate that electrostatics plays a key role in the interactions between CNDs and chloroplast membranes. In the absence of salt, adsorption efficiencies of PEI-CNDs toward model membranes increased with the increase in SQDG concentration, whereas PEI-CNDs did not attach to the model membrane lacking SQDG in detectable amounts (Fig. 3a). This result meets the expectation that negatively

charged SQDG head groups contribute to electrostatic interaction with positively charged PEI-CNDs. To further investigate the role of SQDG in the interaction with CNDs, we determined maximum acoustic mass density ($\Gamma_{QCM\text{-}D}$) of PEI-CNDs on model membranes (Fig. 3b). The absence of SQDG in model membranes led to no significant changes in $\Gamma_{QCM\text{-}D}$; in comparison, SQDG incorporated model membranes induced acoustic mass deposition upon PEI-CND exposure. Increases in adsorption efficiencies with rising SQDG concentration notwithstanding, an increase in the relative abundance of SQDG was found to decrease the maximum $\Gamma_{QCM\text{-}D}$ by PEI-CND adsorption. This decreasing trend in acoustic mass densities indicates that the amount of SQDG is not the only contributor determining PEI-CND incorporation on the model membranes.

Particle-particle repulsion affects capacity of the membrane to accommodate CNDs. Because maximum $\Gamma_{QCM\text{-}D}$ was found to decrease as the SQDG concentration in model membranes increased, we further hypothesized that larger amount of SQDG incorporated into the model membranes leads to stronger interaction with positively charged PEI-CNDs. Nanomaterials with a high affinity for model membranes lead to a decrease in nanomaterial diffusion at the interface.[64,65] Because strongly adsorbed NMs to a surface exhibit a surface exclusion effect on newly adsorbing particles,[66] a tighter adsorption of CNDs on model membrane could lead to reduced particle diffusion at the interface followed by a decrease in CND adsorption. For PEI-CNDs, we found maximum $\Gamma_{QCM\text{-}D}$ to decrease as the SQDG concentration in model membranes increased, which may be the result of PEI-CNDs high affinity for SQDG.

To test our hypothesis that interaction affinity affects the extent of NM adsorption, we first measured changes in energy dissipation during PEI-CND adsorption onto the model membranes (Fig. 3c).[42,53,67] On the 0% SQDG containing model membranes, PEI-CNDs did not cause any significant increases in dissipation to the membrane, whereas incorporation of SQDG into model

membranes induced dissipation change. The extent of dissipation change decreased as SQDG concentration in model membranes increased. The decreasing trend in viscoelasticity suggests that higher SQDG concentration leads to tighter PEI-CND adsorption on the model membranes.

Dissipation changes are often not sufficient to analyze the viscoelasticity of adsorbed layers, because high extent of frequency change may perturb the dissipation of adsorbed layers.[68] To ensure that the observed changes in dissipation stem from the PEI-CND adsorption, we also calculated dissipation change per unit adsorbed mass ($\Delta D/\Delta f$) upon the interaction with the PEI-CNDs (Fig. S5). The decreasing trend of $\Delta D/\Delta f$ with SQDG concentration in model membranes also supports the conclusion that PEI-CND adsorption leads to a decrease in viscoelasticity of the CND-adsorbed interfaces. To further investigate changes in adsorption strength with changes in SQDG relative abundance, we calculated the adsorption stoichiometry between PEI-CNDs and the mass density of SQDG molecules incorporated in the model membranes based on $\Gamma_{QCM\text{-}D}$ as described in Methods. According to the calculation, multiple SQDG molecules appear to be involved in the interactions with PEI-CNDs (Table S1), and the SQDG to PEI-CND ratio increased with increase in SQDG amount. Interactions of both negatively charged CP- and PVP-CNDs with model membranes did not show any detectable frequency or dissipation change. (Fig. S4). Overall, our results indicate that electrostatics plays a key role in the interaction of CNDs with model chloroplast membranes.

The stronger interaction between PEI-CND and the model membranes could lead to a decrease in the trapped water mass associated with the adsorbed PEI-CND.[45] However, we expect that particle-particle repulsion has a larger impact on the change in mass density upon adsorption than the trapped water mass change. The factors determining hydrodynamically coupled (trapped) solvent mass are size, shape, orientation of adsorbates at the interface, monolayer coverage, and

oscillation frequency.[69] In terms of nanomaterial size, the hydrodynamic diameter of PEI-CNDs was almost constant under our experimental conditions. (*circa* 5.3 ± 0.53 nm, *q.v.* Fig. 2e) The CNDs are expected to have spherical shapes, thus the shape and orientation of PEI-CNDs at the interface are not likely to lead to any differences. Another factor governing the extent of hydrodynamically coupled solvent mass is the adsorption strength related to the degree of particle diffusion at the interface.[69] The assessment of viscoelasticity based on ΔD and $\Delta D/\Delta f$ both indicated that higher SQDG content in model membranes led to stronger CND adsorption, thus the probability of particle oscillation, rolling, or sliding could be relatively low. Subsequently, the measured mass densities are likely related to the lateral distribution of CNDs at the surface. We do not expect a large degree of conformational change of PEI-CND and consider our model membranes thin and rigid (Sauerbrey regime, *q.v.* Eq. 3). Under these circumstances, there may not be significant differences in terms of the amount of trapped liquid between weak or strong interaction of PEI-CNDs with the model membranes.

We conclude that both membrane-CND and CND-CND interactions determined CND adsorption onto the model membranes. In the initial stage of CND exposure, negatively charged SQDG molecules in the bilayers governed the extent of positively charged CND interaction with the model membranes. In the later stage of adsorption, higher SQDG content leads to a lower degree of PEI-CND diffusion on the model membranes, which subsequently raises CND-CND repulsion. This increased extent of CND-CND repulsion lowers maximum amount of CND adsorption.

Electrostatics is the primary contributor for CND-model chloroplast membrane interactions. To investigate CND interactions with the model chloroplast lipid membranes under biologically relevant ionic conditions, we employed a gradient of ionic strengths to represent the

plant cytoplasm.[70] We chose KCl, as potassium is the most abundant cation in plant cells. We used 0, 10, and 100 mM KCl, consistent with the optimal range of salt concentration for enzymatic metabolism.[70] As ionic strength increased, the positive ζ-potential of PEI-CNDs was reduced (Fig. 2b), consistent with electrical double layer compression.[71]

Reduced positive ζ-potential of PEI-CNDs was expected to induce weaker electrostatic interaction with SQDG containing model membranes. As expected, adsorption efficiencies of PEI-CNDs onto model membranes decreased as charge screening of attractive electrostatics increased by KCl (Fig. 4). The decreasing trend agrees with the observed change in ζ-potential of PEI-CNDs (Fig. 2b). Under each ionic condition, adsorption efficiencies had the propensity to increase with a rise in SQDG concentration in model membrane. Decrease in ζ-potential of PEI-CNDs reduced lateral repulsion of PEI-CNDs on membrane surfaces, facilitating the higher extent of adsorption. On 5% SQDG containing model membranes, an increase in ionic strength increased $\Gamma_{QCM\text{-}D}$ on the bilayers (Fig. 5a). These results indicate that the membrane capacity for PEI-CNDs is not entirely dependent on initial adsorption efficiency but also related to particle arrangement on membranes. At higher KCl concentrations, there is reduced particle-particle repulsion, resulting in CNDs having a higher packing efficiency at the interface. Changes in ionic strength produced the same effects on 0, 2.5, and 10% SQDG containing model membranes (Fig. S6).

We calculated the fractional surface coverage (θ) to investigate whether the occupied surface area was larger under higher salt condition and to demonstrate PEI-CNDs were well-dispersed on the bilayers without stackings or aggregations. Increases in ionic strength increased the fractional surface coverage area of CNDs, demonstrating that a more packed arrangement of PEI-CNDs on the bilayers stems from a lower extent of particle-particle repulsions (Fig. 5b). Given that the maximum fractional surface coverage area was below 1, PEI-CNDs appeared to be at sub-

monolayer coverage on the model membranes. From the calculated θ, we were also able to speculate the density of PEI-CNDs. The dotted line on Fig. 5b indicates the jamming limit (0.547) mathematically calculated for spherical adsorbates.[54,72] Considering the jamming limit represents zero probability of further adsorption,[73] the density of PEI-CND would be higher than that of polypropylene.

Our results from interactions of CNDs with model chloroplast membranes suggest that the CND–membrane interactions are primarily dictated by electrostatic forces between SQDG and CNDs and between CNDs themselves. Our data also suggest that a random sequential adsorption model (*q.v.* Materials and Methods), which excludes the probability of particle overlapping upon particle introduction to interfaces, explains CND behavior at model lipid membranes over a range of ionic strengths upon initial stage of adsorption.[54,74,75] Anionic CNDs did not lead to detectable interactions over the range of 0 – 100 mM KCl (Fig. S4).

Attachment of PEI-CNDs to the isolated chloroplast. To investigate the influence of ionic strength on the adsorption of positively charged PEI-CNDs to chloroplast membranes, we performed confocal fluorescence microscopy of isolated chloroplasts interfaced with PEI-CNDs under KCl concentrations ranging from 0 to 100 mM (Fig. 6a). The PEI-CNDs have a peak fluorescence emission from 400-550 nm that allows colocalization analysis with isolated chloroplasts from *Arabidopsis thaliana* leaves exhibiting chlorophyll autofluorescence in the range of 650-750 nm (Fig. 6b). The PEI-CND have a quantum yield of 0.43% relative to quinine sulfate (0.1 M, H_2SO_4). The fluorescence intensity of PEI-CNDs increased with higher KCl concentration (Fig. 6c). The highest PEI-CND colocalization with isolated chloroplasts was observed in the 100 mM KCl solution (buffered to pH 7.4 with 10 mM TES buffer). This is consistent with the propensity of PEI-CND adsorption to model chloroplast membranes. From our observation with

isolated chloroplasts, we highlight that ionic strength is an important parameter for PEI-CND interactions with chloroplast biosurfaces. We also confirmed that our model system is a good representation of native chloroplast membranes and can be used to explain NM-chloroplast interactions.

CONCLUSION

We successfully constructed a model system that mimics lipid compositions of chloroplast membranes. We used this model chloroplast membrane to demonstrate that electrostatics is a critical component of the interaction between chloroplast membranes and CNDs. We have reported that a class of sulfur-containing lipids in plastid membranes, SQDG, played an important role in the interaction of model chloroplast membranes with CNDs via electrostatic interactions. We also found that particle-particle repulsion is a critical contributor in determining the extent of CND adsorption to model chloroplast membranes. Due to electrical double layer compression, changes in the ionic environment at CND-chloroplast interface altered the degree of both CND adsorption efficiency to chloroplast membranes and the capacity of chloroplast membranes for adsorbed CND. These results were in accord with a random sequential adsorption model and its dependence on ionic strength of the milieu. We showed that our model chloroplast membrane could elucidate mechanisms of NM adsorption onto native chloroplast membranes. Our study improves understanding of NM–plant organelle interactions at the molecular level by determining the membrane components involved in interactions with NMs, the governing mechanism of the NM-membrane interactions, and the effects of NM physicochemical properties on the interaction with chloroplast membranes. A mechanistic understanding of NM-plant biosurface interactions will

advance rational design rules for NMs with intended targets and/or delivery of chemical and biomolecule cargoes to plant cell organelles.

ACKNOWLEDGEMENT

This work was supported by National Science Foundation under the NSF Center for Sustainable Nanotechnology, CHE-2001611. The NSF CSN is part of the Centers for Chemical Innovation Program.

AUTHOR CONTRIBUTIONS

J.A.P. and J.P.G. conceived the idea. K.K., C.M.A., P.H., S.J., and W.F.B. carried out the experiments. J.A.P. and J.P.G. supervised the research. J.A.P., K.K., and C.M.A. designed the experiments related to QCM-D. K.K., C.M.A., and W.F.B. fabricated lipid bilayers and performed QCM-D experiments. K.K. and J.A.P. interpreted experimental results from the QCM-D experiments. P.H. synthesized the carbon nanodots, and K.K., P.H., and S.J. characterized surface charge and hydrodynamic diameter of carbon nanodots. S.J. performed the confocal microscopy studies with isolated chloroplast and analyzed relevant data. K.K., S.J., J.A.P, and J.P.G wrote the manuscript, and all authors contributed to revising the manuscript.

REFERENCES

1 Y. Shang, M. K. Hasan, G. J. Ahammed, M. Li, H. Yin and J. Zhou, *Molecules*, 2019, 24.

2 P. Hu, J. An, M. M. Faulkner, H. Wu, Z. Li, X. Tian and J. P. Giraldo, *ACS Nano*, 2020, **14**, 7970–

7986.

3 R. Raliya, C. Franke, S. Chavalmane, R. Nair, N. Reed and P. Biswas, *Front. Plant Sci.*, 2016, 7, 1288.

4 A. Avellan, J. Yun, Y. Zhang, E. Spielman-Sun, J. M. Unrine, J. Thieme, J. Li, E. Lombi, G. Bland and G. V. Lowry, *ACS Nano*, 2019, **13**, 5291–5305.

5 I. Santana, H. Wu, P. Hu and J. P. Giraldo, *Nat. Commun.*, 2020, **11**, 2045.

6 F. J. Cunningham, N. S. Goh, G. S. Demirer, J. L. Matos and M. P. Landry, *Trends Biotechnol.*, 2018, **36**, 882–897.

7 S. K. Jat, J. Bhattacharya and M. K. Sharma, *J. Mater. Chem. B*, 2020, **8**, 4165–4175.

8 J. P. Giraldo, M. P. Landry, S. M. Faltermeier, T. P. McNicholas, N. M. Iverson, A. A. Boghossian, N. F. Reuel, A. J. Hilmer, F. Sen, J. A. Brew and M. S. Strano, *Nat. Mater.*, 2014, **13**, 400–408.

9 A. Karny, A. Zinger, A. Kajal, J. Shainsky-Roitman and A. Schroeder, *Sci. Rep.*, 2018, **8**, 1–10.

10 H. Tian, Z. Guo, J. Chen, L. Lin, J. Xia, X. Dong and X. Chen, *Adv. Healthc. Mater.*, 2012, **1**, 337–341.

11 X. Zhao, H. Cui, W. Chen, Y. Wang, B. Cui, C. Sun, Z. Meng and G. Liu, *PLoS One*, 2014, **9**, 2–8.

12 X. Zhao, Z. Meng, Y. Wang, W. Chen, C. Sun, B. Cui, J. Cui, M. Yu, Z. Zeng, S. Guo, D. Luo, J. Q. Cheng, R. Zhang and H. Cui, *Nat. Plants*, 2017, **3**, 956–964.

13 G. S. Demirer, H. Zhang, J. L. Matos, N. S. Goh, F. J. Cunningham, Y. Sung, R. Chang, A. J. Aditham, L. Chio, M. J. Cho, B. Staskawicz and M. P. Landry, *Nat. Nanotechnol.*, 2019, **14**, 456–464.

14 G. V. Lowry, A. Avellan and L. M. Gilbertson, *Nat. Nanotechnol.*, 2019, **14**, 517–522.

15 T. Hofmann, G. V. Lowry, S. Ghoshal, N. Tufenkji, D. Brambilla, J. R. Dutcher, L. M. Gilbertson, J. P. Giraldo, J. M. Kinsella, M. P. Landry, W. Lovell, R. Naccache, M. Paret, J. A. Pedersen, J. M. Unrine, J. C. White and K. J. Wilkinson, *Nat. Food*, 2020, **1**, 416–425.

16 H. Kirchhoff, *New Phytol.*, 2019, **223**, 565–574.

17 Y. Ze, C. Liu, L. Wang, M. Hong and F. Hong, *Biol. Trace Elem. Res.*, 2011, **143**, 1131–1141.

18 H. H. Wang, W. B. Yin and Z. M. Hu, *J. Genet. Genomics*, 2009, **36**, 387–398.

19 H. Daniell, *Biotechnol. J.*, 2006, **1**, 31–33.

20 R. Bock, *Annu. Rev. Plant Biol.*, 2015, **66**, 211–241.

21 G. M. Newkirk, P. de Allende, R. E. Jinkerson and J. P. Giraldo, *Front. Plant Sci.*, , DOI:10.3389/fpls.2021.691295.

22 S. Y. Kwak, T. T. S. Lew, C. J. Sweeney, V. B. Koman, M. H. Wong, K. Bohmert-Tatarev, K. D. Snell, J. S. Seo, N. H. Chua and M. S. Strano, *Nat. Nanotechnol.*, 2019, **14**, 447–455.

23 M. H. Wong, R. P. Misra, J. P. Giraldo, S. Y. Kwak, Y. Son, M. P. Landry, J. W. Swan, D. Blankschtein and M. S. Strano, *Nano Lett.*, 2016, **16**, 1161–1172.

24 M. A. Block, A. J. Dorne, J. Joyard and R. Douce, *J. Biol. Chem.*, 1983, **258**, 13281–13286.

25 J. Barber and K. Gounaris, *Photosynth. Res.*, 1986, **9**, 239–249.

26 P. Moreau, J. J. Bessoule, S. Mongrand, E. Testet, P. Vincent and C. Cassagne, *Prog. Lipid Res.*, 1998, **37**, 371–391.

27 Y. Nakajima, Y. Umena, R. Nagao, K. Endo, K. Kobayashi, F. Akita, M. Suga, H. Wada, T. Noguchi and J.-R. Shen, *J. Biol. Chem.*, 2018, **293**, 14786–14797.

28 D. R. Janero and R. Barrnett, *J. Lipid Res.*, 1981, **22**, 1119–1125.

29 K. Kobayashi, *J. Plant Res.*, 2016, **129**, 565–580.

30 J. Rocha, M. Nitenberg, A. Girard-Egrot, J. Jouhet, E. Maréchal, M. A. Block and C. Breton, *Front. Plant Sci.*, 2018, **9**, 1–7.

31 C. W. Yu, Y. T. Lin and H. min Li, *New Phytol.*, 2020, **228**, 1327–1335.

32 G. Hölzl and P. Dörmann, *Annu. Rev. Plant Biol.*, 2019, **70**, 51–81.

33 M. A. Block, R. Douce, J. Joyard and N. Rolland, *Photosynth. Res.*, 2007, 92, 225–244.

34 A. Cayuela, M. L. Soriano, C. Carrillo-Carrión and M. Valcárcel, *Chem. Commun.*, 2016, **52**, 1311–1326.

35 S. Y. Lim, W. Shen and Z. Gao, *Chem. Soc. Rev.*, 2015, **44**, 362–381.

36 A. Sharma and J. Das, *J. Nanobiotechnology*, 2019, **17**, 1–24.

37 A. Pérez-de-Luque, *Front. Environ. Sci.*, 2017, 5, 12.

38 Y. Wang and A. Hu, *J. Mater. Chem. C*, 2014, **2**, 6921–6939.

39 Q. Zeng, D. Shao, X. He, Z. Ren, W. Ji, C. Shan, S. Qu, J. Li, L. Chen and Q. Li, *J. Mater. Chem. B*, 2016, **4**, 5119–5126.

40 S.-J. Jeon, T.-W. Kang, J.-M. Ju, M.-J. Kim, J. H. Park, F. Raza, J. Han, H.-R. Lee and J.-H. Kim, *Adv. Funct. Mater.*, 2016, **26**, 8211–8219.

41 A. M. Brouwer, *Pure Appl. Chem.*, 2011, **83**, 2213–2228.

42 K. H. Jacobson, I. L. Gunsolus, T. R. Kuech, J. M. Troiano, E. S. Melby, S. E. Lohse, D. Hu, W. B. Chrisler, C. J. Murphy, G. Orr, F. M. Geiger, C. L. Haynes and J. a. Pedersen, *Environ. Sci. Technol.*, 2015, 150812155717009.

43 N. J. Cho, C. W. Frank, B. Kasemo and F. Höök, *Nat. Protoc.*, 2010, **5**, 1096–1106.

44 M. C. Dixon, *J. Biomol. Tech.*, 2008, **19**, 151–158.

45 I. Reviakine, D. Johannsmann and R. P. Richter, *Anal. Chem.*, 2011, **83**, 8838–8848.

46 J. Kankare, *Langmuir*, 2002, **18**, 7092–7094.

47 R. H. Walters, K. H. Jacobson, J. A. Pedersen and R. M. Murphy, *J. Mol. Biol.*, 2012, **421**, 329–347.

48 A. C. Mensch, R. T. Hernandez, J. E. Kuether, M. D. Torelli, Z. V. Feng, R. J. Hamers and J. A. Pedersen, *Environ. Sci. Technol.*, 2017, **51**, 11075–11084.

49 M. Zhang, J. Soto-Rodríguez, I. C. Chen and M. Akbulut, *Soft Matter*, 2013, **9**, 10155–10164.

50 M. Zhang and M. Akbulut, *Langmuir*, 2011, **27**, 12550–12559.

51 W. S. Cleveland and S. J. Devlin, *J. Am. Stat. Assoc.*, 1988, **83**, 596–610.

52 K. H. Jacobson, T. R. Kuech and J. A. Pedersen, *Environ. Sci. Technol.*, 2013, **47**, 6925–6934.

53 E. S. Melby, A. C. Mensch, S. E. Lohse, D. Hu, G. Orr, C. J. Murphy, R. J. Hamers and J. A. Pedersen, *Environ. Sci. Nano*, 2016, **3**, 45–55.

54 Z. Adamczyk and P. Weroński, *J. Chem. Phys.*, 1996, **105**, 5562–5573.

55 J. J. Kelley, M. L. Jespersen and R. A. Vaia, *J. Nanoparticle Res.*, , DOI:10.1007/s11051-018-4388-y.

56 L. Jiang, C. Zou, Z. Zhang, Y. Sun, Y. Jiang, W. Leow, B. Liedberg, S. Li and X. Chen, *Small*, 2014, **10**, 609–616.

57 D. I. Arnon, *Plant Physiol.*, 1949, **24**, 1–15.

58 M. A. Brown, Z. Abbas, A. Kleibert, R. G. Green, A. Goel, S. May and T. M. Squires, *Phys. Rev. X*, 2016, **6**, 1–12.

59 M. Nedyalkova, S. Madurga, S. Pisov, I. Pastor, E. Vilaseca and F. Mas, *J. Chem. Phys.*, , DOI:10.1063/1.4762830.

60 M. Voronova, N. Rubleva, N. Kochkina, A. Afineevskii, A. Zakharov and O. Surov, *Nanomaterials*, , DOI:10.3390/nano8121011.

61 K. M. Koczkur, S. Mourdikoudis, L. Polavarapu and S. E. Skrabalak, *Dalt. Trans.*, 2015, **44**, 17883–17905.

62 L. Trotsiuk, A. Antanovich, A. Lizunova and O. Kulakovich, *Colloid Interface Sci. Commun.*, 2020, **37**, 100289.

63 A. N. Kuskov, P. P. Kulikov, A. V Goryachaya, M. N. Tzatzarakis, A. M. Tsatsakis, K. Velonia and M. I. Shtilman, *J. Appl. Polym. Sci.*, 2018, **135**, 45637.

64 Y. K. Lee, S. Kim, J. W. Oh and J. M. Nam, *J. Am. Chem. Soc.*, 2014, **136**, 4081–4088.

65 P. Chen, Z. Huang, J. Liang, T. Cui, X. Zhang, B. Miao and L. T. Yan, *ACS Nano*, 2016, **10**, 11541–11547.

66 P. Schaaf, J.-C. Voegel and B. Senger, *J. Phys. Chem. B*, 2000, **104**, 2204–2214.

67 C. A. Lochbaum, A. K. Chew, X. Zhang, V. Rotello, R. C. Van Lehn and J. A. Pedersen, *ACS Nano*, 2021, **15**, 6562–6572.

68 F. Höök, M. Rodahl, P. Brzezinski and B. Kasemo, *Langmuir*, 1998, **14**, 729–734.

69 Z. Adamczyk and M. Sadowska, *Anal. Chem.*, 2020, **92**, 3896–3903.

70 P. Ragel, N. Raddatz, E. O. Leidi, F. J. Quintero and J. M. Pardo, *Front. Plant Sci.*, , DOI:10.3389/fpls.2019.00281.

71 A. V. Delgado, F. González-Caballero, R. J. Hunter, L. K. Koopal and J. Lyklema, *J. Colloid Interface Sci.*, 2007, **309**, 194–224.

72 J. J. Kelley, M. L. Jespersen and R. A. Vaia, *J. Nanoparticle Res.*, 2018, **20**, 290.

73 P. Viot, G. Tarjus, S. M. Ricci and J. Talbot, *J. Chem. Phys.*, 1992, **97**, 5212–5218.

74 E. A. M. Brouwer, E. S. Kooij, H. Wormeester and B. Poelsema, *Langmuir*, 2003, **19**, 8102–8108.

75 D. García Raya, C. Silien, M. Blázquez, T. Pineda and R. Madueño, *J. Phys. Chem. C*, 2014, **118**, 14617–14628.

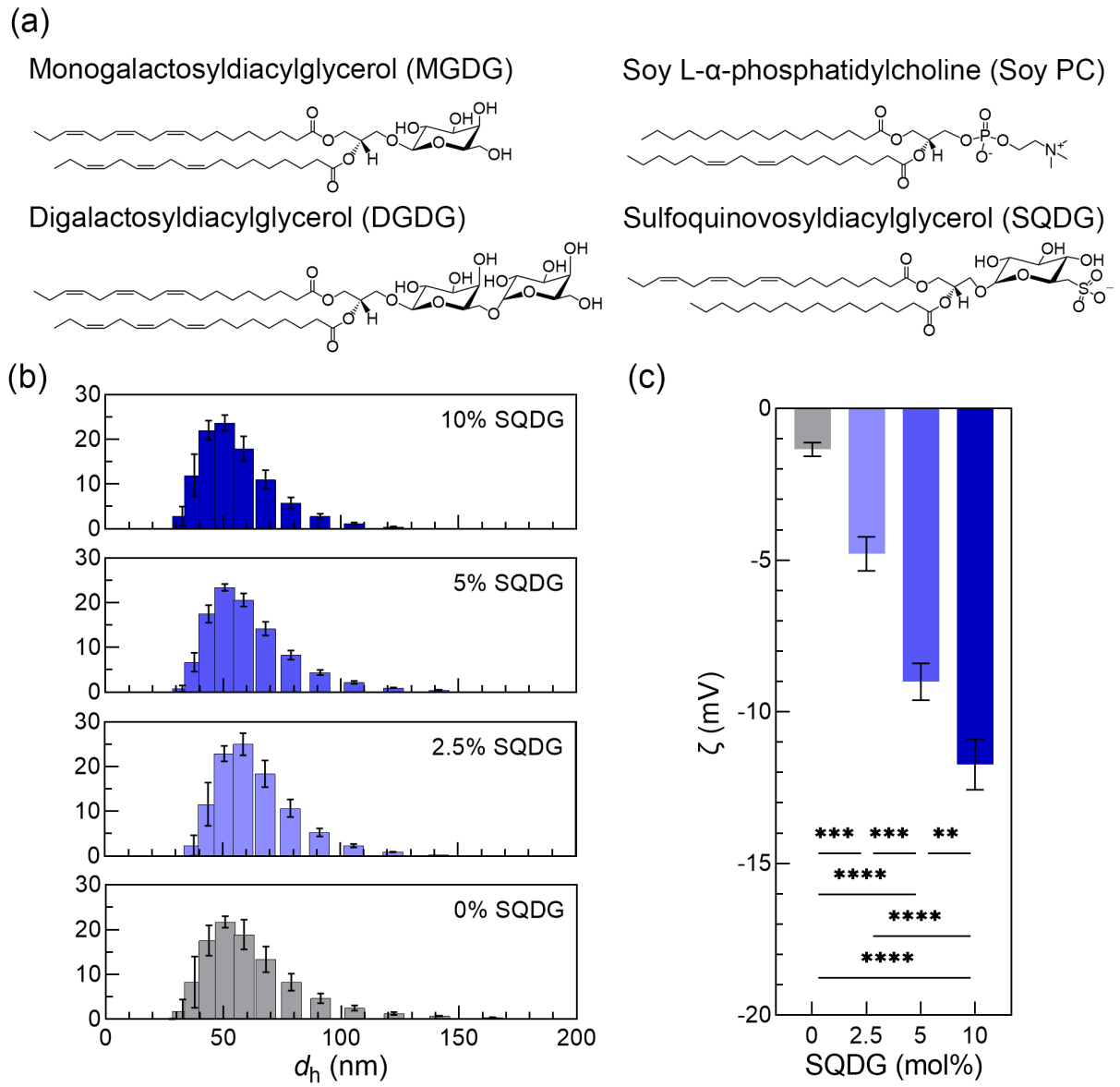

Figure 1. (a) Representative chemical structure of lipids composing model chloroplast membranes. The content of SQDG varied from 0 to 10 mol%. (b) Hydrodynamic diameters (d_h) and (c) zeta potential (ζ) of unilamellar vesicles containing 0, 2.5, 5, and 10 mol% SQDG. Each vesicle solution was diluted to a concentration of 10 μg·mL^{-1} in 10 mM $MgCl_2$ buffered to pH 7.5 with 10 mM HEPES for the measurements. Bars indicate mean values, and error bars are one standard deviations from three replicates. Vesicle hydrodynamic diameter did not differ for the range of SQDG contents examined ($p > 0.05$). Analysis of variance showed that the effect of SQDG content on the zeta-potential of lipid vesicles was significant, F (3, 8) = 135.5, $p < 0.0001$. Tukey post-hoc tests revealed that each group differed from the others. **, $p < 0.01$; ***, $p < 0.001$; ****, $p < 0.0001$

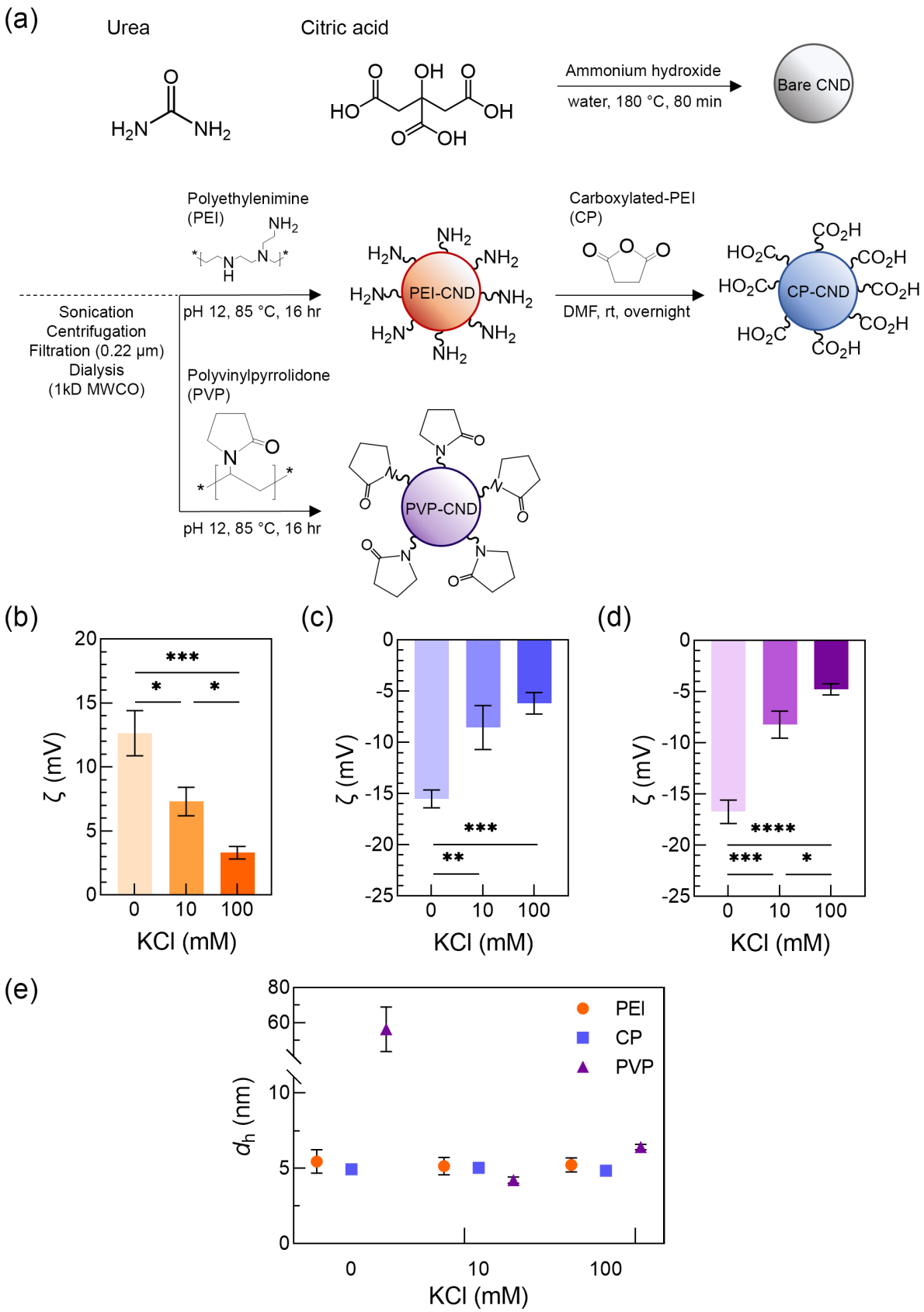
(a)
Urea
Citric acid
Ammonium hydroxide
water, 180 °C, 80 min
Bare CND
Polyethylenimine
(PEI)
Sonication
Centrifugation
Filtration (0.22 μm)
Dialysis
(1kD MWCO)
pH 12, 85 °C, 16 hr
PEI-CND
Carboxylated-PEI
(CP)
DMF, rt, overnight
CP-CND
Polyvinylpyrrolidone
(PVP)
pH 12, 85 °C, 16 hr
PVP-CND
(b)
ζ (mV)
KCl (mM)
(c)
ζ (mV)
KCl (mM)
(d)
ζ (mV)
KCl (mM)
(e)
d_h (nm)
KCl (mM)
PEI
CP
PVP

Figure 2. (a) Synthesis protocol and structure of surface modification on CNDs. We synthesized 3 different types of CNDs having different surface charges/hydrophobicities. Zeta potentials of (b) PEI-, (c) CP-, and (d) PVP-CNDs and (e) hydrodynamic diameters (d_h) of them were measured under 0-100 mM of ionic strengths adjusted by KCl. Each CND suspension was diluted to a concentration of CNDs corresponding to UV absorbance of 1.2037 at 410 nm, in 0-100 mM KCl buffered to pH 7.5 with 10 mM HEPES for the measurements. Bars indicate mean values, and error bars are one standard deviations from three replicates. Only PVP-CNDs under salt-free condition aggregated. From zeta potential measurements, analysis of variance showed that the effect of electric double layer compression by salts. Changes in zeta-potential of CNDs were statistically significant. For PEI-, CP-, and PVP-CNDs, F (2, 6) = 29.09, p = 0.0008, F (2, 6) = 32.09, p = 0.0006, and F (2, 6) = 102.1, $p < 0.0001$, respectively. Tukey post-hoc tests revealed that each group differed from the others. *, $p < 0.05$; **, $p < 0.01$; ***, $p < 0.001$; ****, $p < 0.0001$

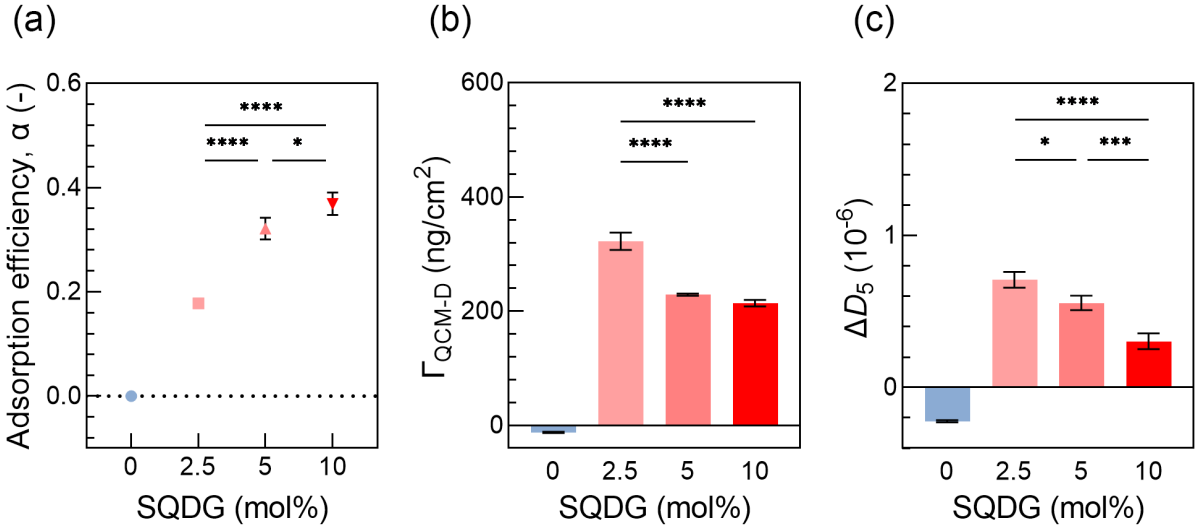

Figure 3. (a) Adsorption efficiency of PEI-CNDs on 0 – 10% SQDG containing bilayers. The adsorption efficiency on 0% SQDG bilayer was considered zero because PEI-CND did not cause detectable changes in frequency upon the exposure. (b) Changes in acoustic mass density upon PEI-CND exposure decrease with an increase in SQDG content. (c) Dissipation change of 5th harmonic shows increasing SQDG concentration leads to more rigid adsorption. Measurements were conducted in 10 mM HEPES (pH 7.5). Error bars on each graph indicate the standard deviation of triplicate measurements. An analysis of variance followed by Tukey post-hoc tests revealed that each group is statistically different from the others. Significance of differences: *, $p \leq 0.05$; ***, $p \leq 0.001$; ****, $p \leq 0.0001$.

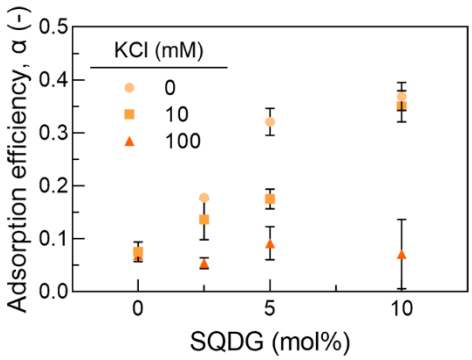

Figure 4. Adsorption efficiencies of PEI-CNDs on 0 – 10% SQDG containing bilayers under 0 -100 mM KCl.

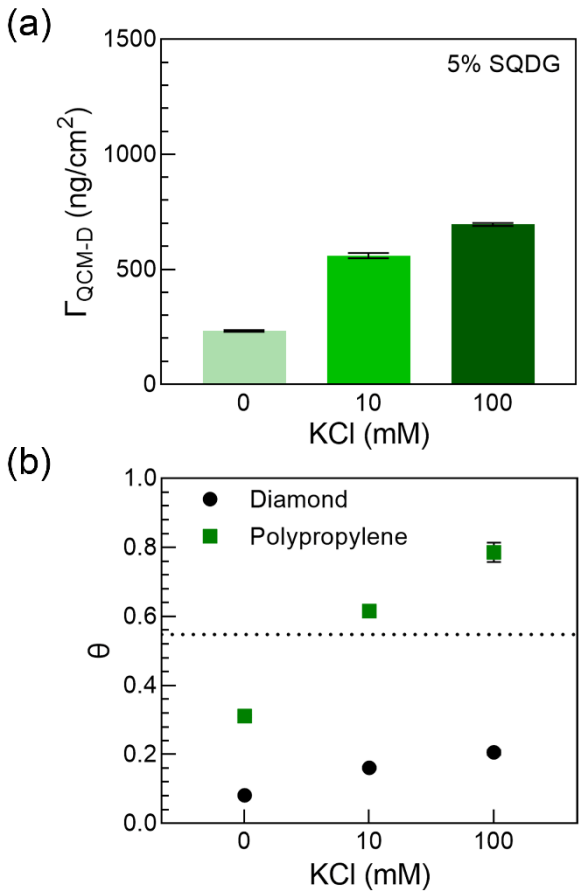

Figure 5. (a) Acoustic surface mass densities and (b) fractional surface coverages, θ, for bilayers containing 5% SQDG. The assumptions used to calculate fractional surface coverages is described in Methods. The dotted line represents jamming limit, 0.547.

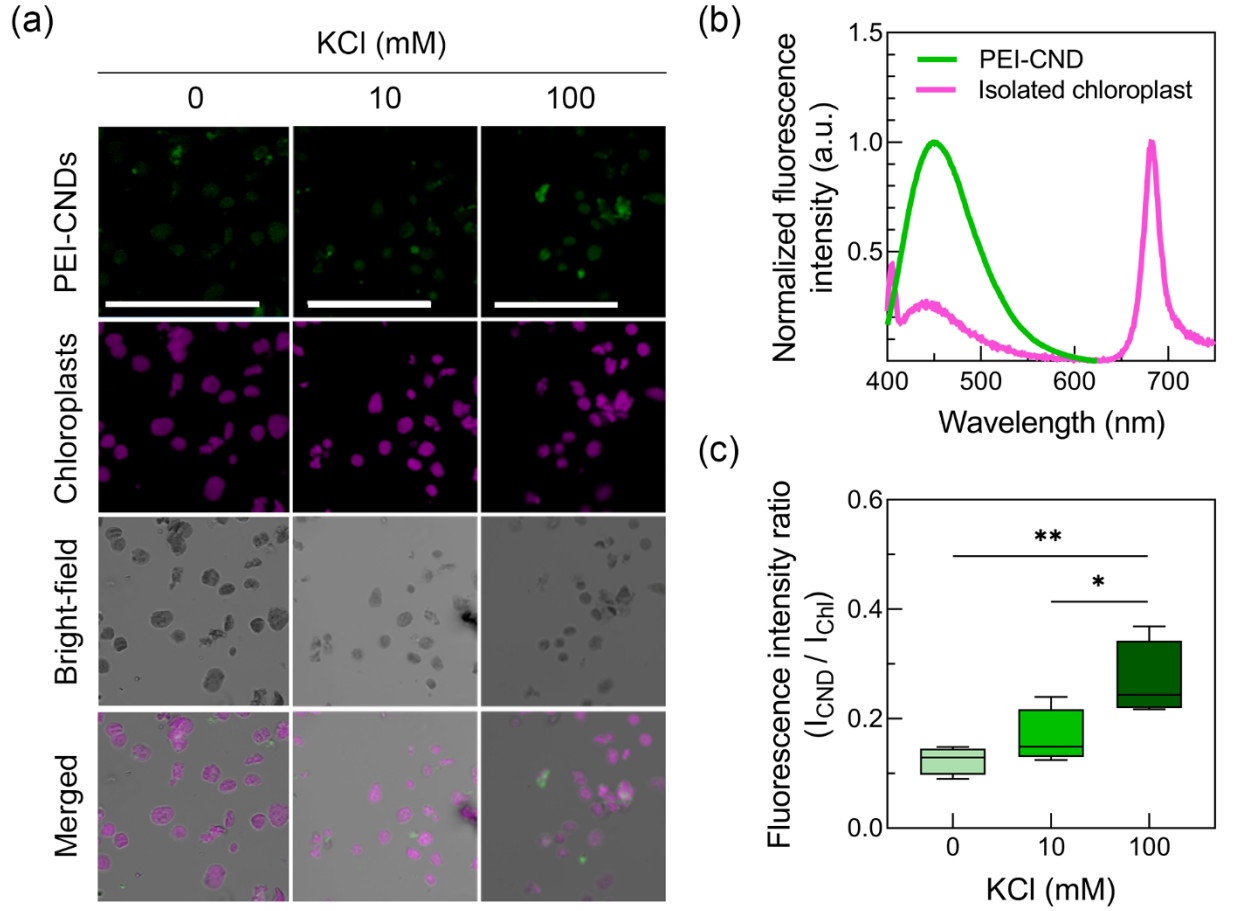

Figure 6. Interactions of positively charged PEI-CNDs with chloroplasts is dependent on the ionic strength of the medium. (a) Representative confocal images of PEI-CNDs interfaced with isolated chloroplasts under increasing concentration of KCl (0-100 mM). Scale bar, 50 μm. (b) Fluorescence spectra of PEI-CNDs and *Arabidopsis thaliana* leaves upon 405 nm excitation. (c) Mean fluorescence intensity values of PEI-CNDs normalized by chloroplast autofluorescence intensity. Normalized PEI-CND fluorescence intensity increases with the KCl concentration indicating higher affinity with chloroplasts under enhanced ionic strength. Error bars on each graph indicate the standard deviation of five replicates. An analysis of variance followed by Tukey post-hoc tests revealed that each group is statistically different from the others. Significance of differences: *, $p \leq 0.05$; **, $p \leq 0.01$.